7/6/78

CONF-781202--9

PREPRINT UCRL-80645

# Lawrence Livermore Laboratory

MODELING VERTICAL LOADS IN POOLS RESULTING FROM FLUID INJECTION

W. Lai, E. W. McCauley

15 June 1978

This paper was prepared for submission to the Symposium on Fluid Transient and Acoustics in the Power Industry at the 1978 Winter Annual Meeting, ASME, San Francisco, California December 10-15, 1978



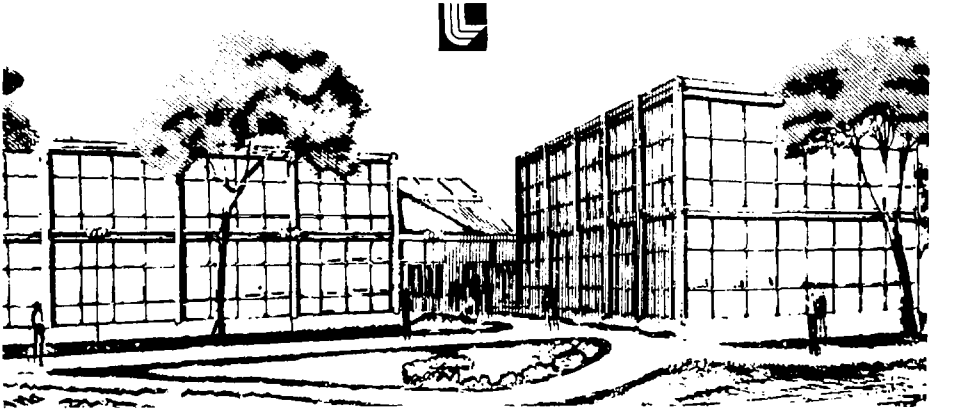

# MODELING VERTICAL LOADS IN POOLS RESULTING FROM FLUID INJECTION

W. Lai and E. W. McCauley

University of California, Lawrence Livermore Laboratory
P.O. Box 808, Livermore, California 94550

ABSTRACT

Table-top model experiments were performed to investigate pressure suppression pool dynamics effects due to a postulated loss-of-coolant accident (LOCA) for the Peachbottom Mark I boiling water reactor containment system. The results guided subsequent conduct of experiments in the 1/5-scale facility and provided new insight into the vertical load function (VLF).

Model experiments show an oscillatory VLF with the download typically double-spiked followed by a more gradual sinusoidal upload. The load function contains a high frequency oscillation superimposed on a low frequency one; evidence from measurements indicates that the oscillations are initiated by fluid dynamics phenomena.

The maximum download diminishes with initial downcomer fill level. When the downcomer is initially empty, the maximum download degenerates to a gradual sinusoidal shape. This leads to the possibility of an empirical model of the VLF consisting of damped low frequency and a higher frequency (v10 times the low frequency) sinusoidal components.

As evidenced by the 25 air-water tests conducted with our 1/5-scale three-dimensional facility, the VLF measured from the table-top experiments accurately predicted the general characteristics of the VLF from larger, properly configured apparatus.

## INTRODUCTION

The success of the pressure suppression containment system design of a boiling water reactor (BWR) is dependent on the capability of a water heat sink to provide rapid and stable condensation of the released primary coolant during a hypothetical loss-of-coolant accident (LOCA). During the initial stage of the LOCA, significant vertical loads due to noncondensable air injection from the drywell are imposed on the toroidal wetwell. To gain a better understanding of the dynamic behavior of the system, a 1/5-scale three-dimensional pressure suppression experimental facility was developed for the Nuclear Regulatory Commission (NRC)(Fig.1).[1] Extensive testing was performed to quantify the hydrodynamic phenomena and associated forces.

Prior to the 1/5-scale tests, however, an inexpensive but extensive series of table-top experiments were used to investigate the fluid dynamics of the system. These small-scale experiments provided detailed phenomenological and theoretical understanding of the key features of the dynamic behavior of the pressure suppression system. The results accurately predicted the later observed transient hydrodynamically-induced load function for the large-scale facility.

The objective of this paper is to characterize the vertical load function from table-top investigations that were conducted prior to the 1/5-scale tests (1,2).

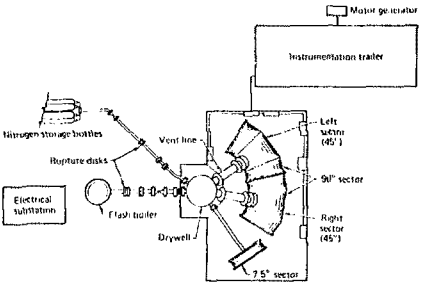


Fig. (1a) Plan View

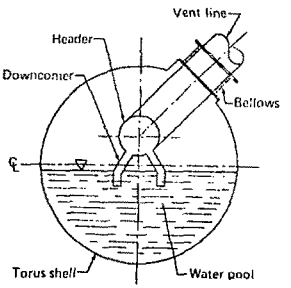


Fig. (1b) Torus System

Fig. 1. Schematic of 1/5-Scale Pressure Suppression Experiment Facility

The small size of the apparatus and the indoor environment of the table-top experiments permitted good control of test conditions and rapid achievement of highly specialized results. In addition, the results of the table-top studies are related to the results from the 1/5-scale torus experiment

[1]Work performed for the United States Nuclear Regulatory Commission contract 109A:A-118-6, under the auspices of the U.S. Department of Energy by the Lawrence Livermore Laboratory under contract number W-7405-Eng-48.

EXPERIMENTAL DESIGN

Laboratory generation of the VLF requires modeling of the controlling physical phenomena; i.e., the dynamics of vent clearing, bubble growth, and pool rise must be preserved. Total geometric similarity is of secondary importance unless scalability is required. For these and cost considerations, the characterization experiments were conducted with apparatus which consisted of a single, glass downcomer in a spherical flask (a standard boiling flask) half filled with water (Fig. 2). The size and submergence ratios were geometrically scaled from plant size.[2] This use of partial geometric scaling was a deliberate attempt to limit the number of variables to be investigated. The apparatus was scaled 1/33.4 of the Peachbottom BWR. Because of incomplete modeling, the measurements (e.g., peak forces) are not applicable to full size plants. However, it was anticipated that observed dynamic phenomena would be representative of that to be expected in large scale tests or full size plants.

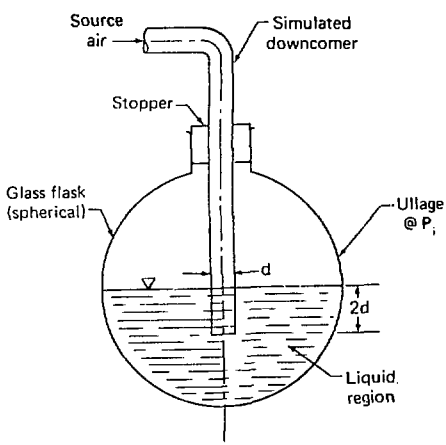


Fig. 2. Cross-Section of Bench Top Downcomer/Flask System

The downcomer/flask system is supported by a strut assembly (3-legged) from a load cell secured to a horizontal crossbeam. The beam ends are firmly fastened to vertical rods attached to a metal table. Vibration characteristics of the support system were investigated systematically to insure absence of support structure resonances in the VLF frequencies of interest (1,2). Oscillations were excited by a hammer blow. Those frame components found to exhibit excitable frequencies near observed oscillations in typical VLF's were selectively stiffened to permit separation of effects. The results of tests reported here were conducted with the stiffened assembly. However, it was shown in Ref. 1 and 2 that the VLF's from the stiffened and original experimental apparatus differed only in degree of damping of high frequency oscillations.

Tests were conducted with the initial ullage air space partially evacuated. The downcomer was isolated from ambient pressure air by a direct acting solenoid valve. The glass apparatus permitted cinematography of the transient events following solenoid opening; the water was dyed for photographic enhancement. The pool, and acceleration of the support were recorded simultaneously with oscilloscopes (Fig. 3). The maximum driving to flask ullage pressure ratio used in these studies was 3:1.

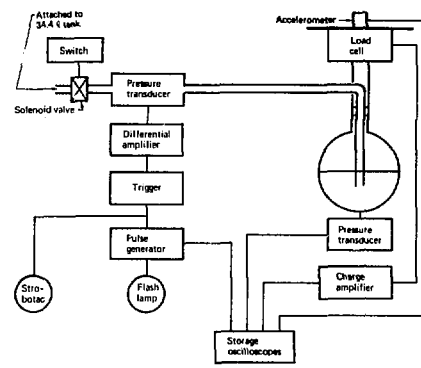


Fig. 3. Schematic of Experimental Apparatus.

RESULTS AND DISCUSSIONS

Listed in Table 1 are selected data from three series of tests. The variations exhibited by the data are attributable to inaccuracies in setting the initial conditions. For most of the tests listed in Table 1, the crossbeam acceleration at midspan, the dynamic load, and the pressure at the bottom of the flask were simultaneously recorded. All transducers were oriented to measure vertically along the axis of the downcomer.

Figure 4 is a set of typical oscilloscope records of the dynamic event. The nature of four specific features are of particular interest in the VLF:

- The double peak download.
- The maximum upload.
- The damped sinusoid carrier wave following the peak upload.
- The damped high frequency sinusoid superimposed on the carrier wave.

The Double Peak Download

Although a download is expected from downcomer clearing, it was not intuitively clear that the download should be spiked, especially not the distinctive double spikes (Fig. 4). The oscilloscopes are triggered by initiation of gas flow into the downcomer. The VLF traces show a long delay before the initial download peak appears abruptly followed quickly by the second

[2] The apparatus used in these experiments was a modification of that designed by F. A. Morrison (3).

peak; Fig. 4, a typical VLF trace for an initially full downcomer, shows a 16 ms delay to the first peak and ∿1.5 ms between first and second peaks. The duration of the time delay decreases with downcomer fill level; this effect is discussed in a later section of this paper.

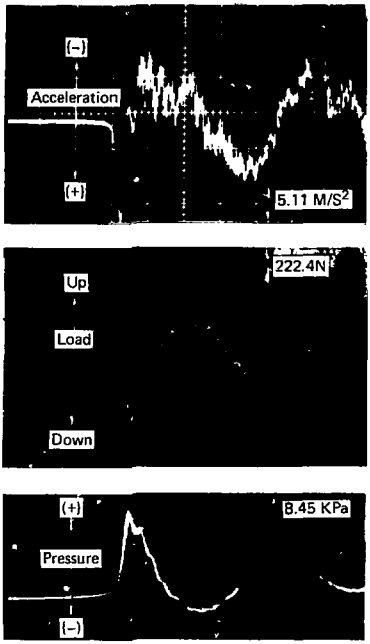


All time scale 5 ms/cm

Fig. 4. Typical Dynamic Records of Table Top.

If we assume that the impulsive download peaks are both flow induced, then from Newton's second law, the flow momentum must change abruptly. The gas flowing into the downcomer must pressurize the space sufficiently to overcome the friction and static head before pushing the water out of the downcomer; this is the compression stage discussed in Ref. 4.[3] Once started, the water accelerates out of the downcomer transferring its momentum to the wall which induces the first download pulse. Figure 5 is a typical plot of the position of the water-air interface in the downcomer as a function of time; the data was measured from projections of high speed movie frames. The slope of the curve in Fig. 5 is the velocity and, of course, the change in slope is the acceleration of the interface. The rapid change in velocity as the water is expelled has the requisite qualities to induce an abrupt load, the first spike of the download.

Following the first download pulse, the high speed movie [illegible]as the sudden growth of a bubble. From measurements gas flow in the downcomer (4) (Fig. 6), the gas flow [illegible] doubles in ∿2 ms during bubble initiation. This rapid change in gas flow rate implies a momentum rate exchange consistent with an impulsive load, the second peak of the double download.

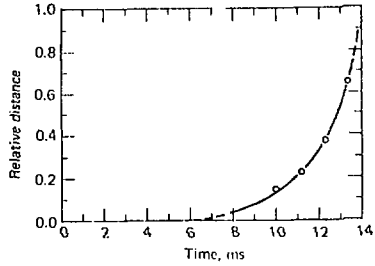


Fig. 5. Typical Water-air Interface Position in the Downcomer as a Function of Time During Downcomer Clearing.

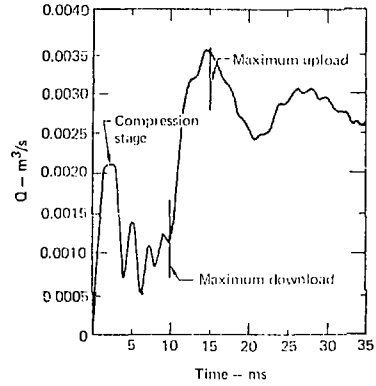


Fig. 6. Typical Air Flow Rate in the Downcomer as a Function of Time During Downcomer Clearing.

The Maximum Upload

The maximum upload is attributed to the combined effects of pool levitation and of ullage compression due to pool rise. The force due to levitation alone may be estimated from the pressure differential between air space and pool bottom (Fig. 7a). The differential pressure is assumed to decrease linearly to a minimum value near the pool surface; the minimum, suggested by published data (5,6), is assumed to be 85% of the maximum value which occurs directly below the downcomer. The force due to ullage compression alone may also be estimated by calculating the isothermal pressure rise in the hemispherical volume of gas as the volume decreases due to pool rise (Fig. 7b).

[3] The compression stage of downcomer clearing is indicated in Fig. 6.

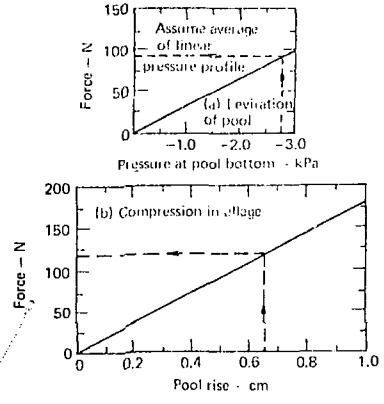


Fig. 7. Estimated Forces due to (a) Levitation and (b) Compression

Careful analysis of high speed movies for 15/5 pressure ratio tests show that the average pool rise at maximum upload is between .51 and .76 cm. The average rise is estimated during the prominent, rapid bulging of the pool surface by the downcomer which precedes the later more gradual rise of the entire pool surface. Figure 7b shows that a pool rise of .66 cm will cause an 120N upload. Table 1 shows that the pressure at the bottom of the flask at maximum upload varies between -2.0 to -3.3 kPa for 15/5 pressure ratio tests. A change of -2.8 kPa will result in an upforce of 93N (Fig. 7a). The sum of these loads is 213N which is the same magnitude as that measured for the 15/5 tests. These data show that the maximum upload can result from a combination of pool levitation and ullage compression.

The Damped Carrier Wave

Examination of the average carrier (or low) frequencies listed in Table 1 shows that the frequencies increase with ullage pressure (Fig. 8). Compressing the time scale on the oscilloscope shows that these low frequency oscillations damp out rapidly (Fig. 9); except for the time scale, the test conditions for Figs. 4 and 9 are the same. These observed effects are consistent with air-water interactions as discussed below.

Note in Fig. 9 that the accelerometer trace shows the beam vibrating after the pressure and VLF have essentially damped out; disruption of the pool surface begins ~20 msec after the maximum download. That the beam is vibrating after the pressure and VLF signals have essentially damped out shows that structural interaction has no effect on the oscillating behavior of the pressure and VLF traces. Instead, Fig. 9 shows that the crossbeam is reacting sympathetically to the dynamic loads. The distortions in the pressure trace from a smooth sinusoid, especially in the tail portion of the pressure trace, are attributed to pool splash. In addition to the pressure fluctuations, the pressure in the flask rises steadily due to the continuous flow of gas into the flask. This effect is exhibited in the pressure trace by the gradual positive shift in the base pressure line with time.

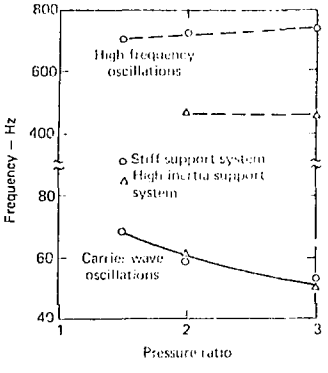


Fig. 8. Effect of Ullage Pressure on Audio Oscillation Frequencies.

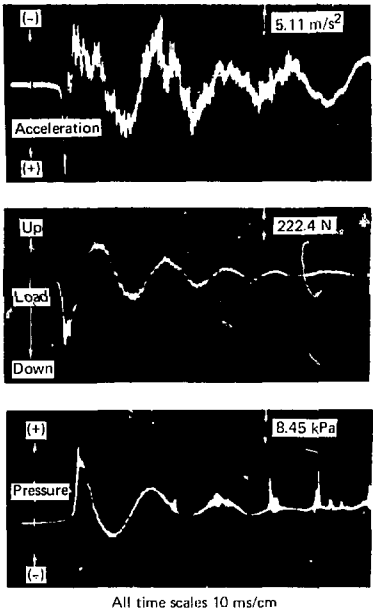


Fig. 9. Typical Dynamic Response Traces Showing the Rapid-Damping of the Pool Disturbances

The magnitude of oscillations of the dynamic events suggest that the [illegible] observable. With this in mind, high speed movies were examined critically. The examination confirmed that

the oscillating carrier wave results from air-water interactions arising from vertical oscillations of the bubble. During the course of expansion, the bubble dynamically adjusts to the pool confinement and continuing air injection by oscillating vertically much as a piston. Plotting the motion picture frame numbers (equivalent to time) corresponding to the high and the low positions of the bubble onto the VLF shows a 1 to 1 correspondence between bubble position and load (Fig. 10); the slight mismatch results primarily from the discrete frames available (900 frames/second).

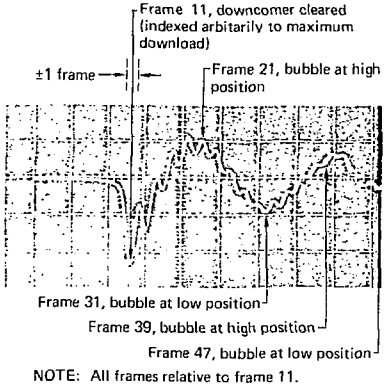


NOTE: All frames relative to frame 11.

Fig. 10. Correspondence Between Bubble Position and Carrier Oscillations.

Vertical oscillations of the bubble are also observed at lower test pressure ratio. The frequency of bubble oscillations (i.e., frequency of the carrier wave) tabulated in Table 1, plotted in Fig. 8, shows that the frequency increases with ullage pressure. As previously stated, this is the expected trend for air-water interaction.

The Damped High Frequency Oscillations

The high frequency oscillations seem to be initiated by the second peak of the double spike download. The average values of the high frequency oscillations listed in Table 1, plotted in Fig. 8 are essentially independent of ullage pressure. Figure 8 shows ~5% decrease when the ullage pressure is doubled.

Careful examination of the three dynamic response traces such as Fig. 4, shows near perfect correspondence among high frequency oscillations. The oscillations are also phased properly, i.e., a download gives rise to a down acceleration and an increase in pressure. Unfortunately, the high frequency oscillations in the acceleration trace after the second peak is hidden in higher amplitude Khz level oscillations.

Although attributing high frequency oscillations to structural support interaction is tempting, it is difficult to conceive of an interaction that would result in synergistic, in-phase response between load and pressure at the bottom of the flask.

AN EMPIRICAL VLF MODEL

Figures 11 to 13 show oscilloscope traces from table-top experiments to determine the effect of downcomer fill level on the VLF (7). The increased relative magnitude of the second pulse when downcomer fill level is reduced to 80% is clearly shown in Fig. 11. The VLF for progressively lower initial downcomer fill levels are shown in Fig. 12; the trace for 80% full is repeated to provide an index for comparison. Note that the time between the first and second download peaks remain constant at ~1.5 ms, even as the second pulse becomes dominant (note the trace for 60%). Figure 13 exhibits the same trends at a lower pressure ratio. Figures 11 to 13 also show that the time duration of the first download (the composite pulse measured along the baseline) remains essentially constant at ~3 ms regardless of the initial downcomer fill level.

The characteristic double spiked maximum download observed with a full downcomer has changed to a residual sinusoidal download for the initially empty downcomer. Note that the phase relationship observed in these flask tests between load peaks and acceleration of the center of the flask support beam is that of the load driving the beam and this is maintained regardless of the downcomer fill level (Figs. 14 and 15).

These data suggest an empirical VLF model composed of two damped sinusoids as illustrated in Fig. 16. The peak loads, frequencies, oscillations, and damping constants must be determined from experimental data.

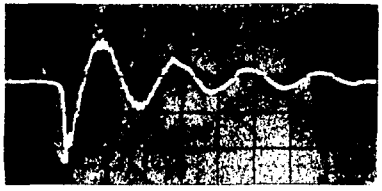

Downcomer initially full

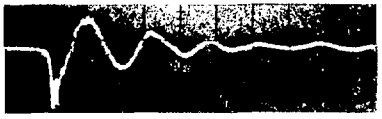

Downcomer initially 80% full

Vertical scale = 222.4 N/cm

Horizontal scale = 10 ms/cm

Fig. 11. Comparison of VLF's for an Initially Full Downcomer and for an Initially 80% Full Downcomer (pressure ratio = .11).

COMPARISON WITH VLF FROM 1/5-SCALE LLL[4] EXPERIMENTS (6)

The results of the table-top VLF characterization study are summarized in Fig. 17. The general distinguishing features of the VLF from table-top experiments are also observed in the RVLF (response VLF) and HVLF (hydrodynamic VLF) from the 1/5-scale experiments (Fig. 18). This is not proof that identical mechanisms are operative in all experiments. The RVLF is measured with load cells. The HVLF is obtained by integration of pressure measurements so that the pressure traces are also oscillatory (Fig. 19). The pressure measurements

[4] LLL = Lawrence Livermore Laboratory.

in Ref. 8 show the same type of oscillatory behavior (Fig. 20).

Note the characteristic double pulse download in Fig. 18. The second spike of the double download was identified as hydrodynamically induced by Davis in a preliminary study with a linear momentum model (9). Lai (6) clarified and extended Davis' analysis to support the hydrodynamic nature of the double spike download. An important aspect of Lai's analysis was the HVLF for the 7.5° torus sector (Fig. 21). The 7.5° torus sector is much stiffer than the 90° sector[5] (10) but in spite of this, the time between the double pulse is about the same (compare Fig. 18 and 21).

A major component of the maximum upload for the 1/5-scale experiment is pool impact of the header. If the flask experiments were conducted with a simulated header, pool impact would occur virtually ahead of the time observed for the maximum upload due to pool levitation and ullage compression. From high speed movies and header impact accelerometers, the time and duration of the maximum upload due to header impact for the 1/5-scale experiment is readily identified (Fig. 18). The maximum header impact load distorts the maximum upload portion of the damped carrier wave of the proposed empirical VLF model but in reality also to the model.

Cinematography for the 1/5-scale experiment was conducted through six inch diameter ports. During filming of pool dynamics, these ports were rapidly obscured by pool splash or by bubbles. For this reason, the high speed movies cannot provide the visual observation that could identify the source of the carrier

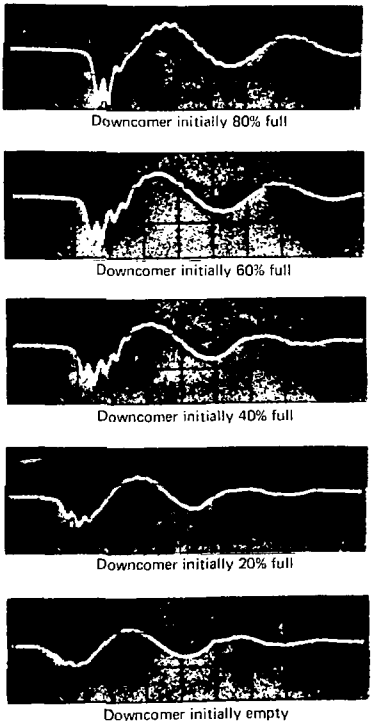


Fig. 12. Effect of Initial Downcomer Fill Level on the VLF (pressure ratio = 3:1).

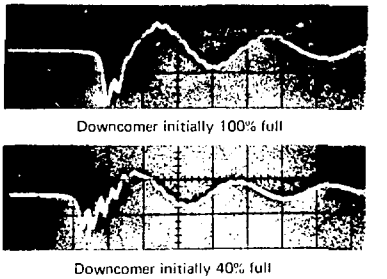


Fig. 13. Effect of Initial Downcomer Fill Level on the VLF (pressure ratio = 3:1).

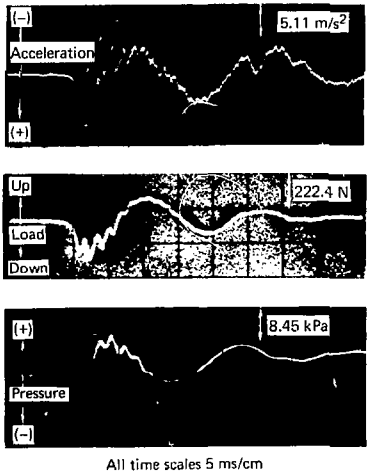


Fig. 14. Typical Dynamic Records for Initial Downcomer Fill Level of 40% Full (pressure ratio = 3:1).

[5] The 1/5-scale LDL experiments were conducted in a facility which permitted simultaneous testing in a 7.5° torus sector and a 90° torus sector (Fig. 1a).

wave oscillations.

The high frequency oscillations in the 1/5-scale 90° torus VLF (Fig. 18) initiated by the second download spike, result from structural interaction (6). The observed high frequencies appear to be apparatus dependent; the EVLF for the stiffer 1/5-scale 7.5° torus contains higher frequency components (compare Fig. 18 and 21).

*CONCLUSIONS*

The table-top flask experiments accurately predicted the general characteristics of the VLF for larger, properly configured apparatus. Specifically, the table-top experiments showed that

(1) the hydrodynamically induced vertical load function is double peaked.

(2) the maximum upload results from levitation of the pool and compression of the ullage. (Though the flask experiments lack a header, header impact adds a significant component to the maximum upload).

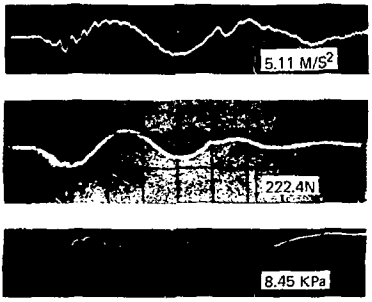


Fig. 15. Typical Dynamic Records for Initially Empty Downcomer (pressure ratio = 3:1).

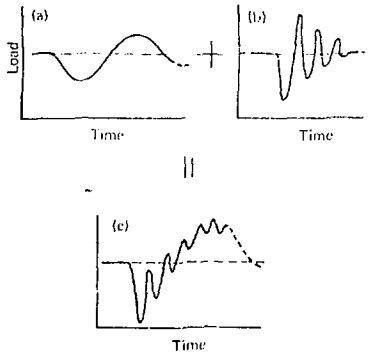


Fig. 16. Empirical Vertical Load Function Model.

(3) the carrier wave oscillations of the VLF for table-top experiments are induced by vertical oscillations of the bubble.

(4) The hydrodynamically induced second download spike excites vibrations which can be identified as structural in both table-top apparatus and in the 1/5-scale 90° torus VLF.

(5) An empirical model of the VLF can be constructed by adding two damped sinusoidal functions. The maximum amplitudes, frequencies, and damping constants must be derived from experimental data. Header impact load, also from experiments, may be added.

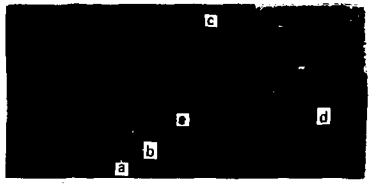


Fig. 17. Summary of VLF characteristics for table-top experiments. (a) Hydrodynamic origin: peak downforce results from ejection of water slug into the pool. (b) Hydrodynamic origin: second peak of downforce becomes dominant as downcomer initial fill level is reduced. (c) Hydrodynamic origin: maximum upforce given by average, [illegible] combination of pool levitation and compression due to pool swell). (d) Hydrodynamic origin: low frequency carrier wave due to *vertical* oscillations of the expanding air bubble. Frequency increases with ullage pressure. Oscillations are in phase with pressure oscillations at bottom of pool. (e) Hydrodynamic origin: high frequency on carrier wave not fully characterized; slight reduction with increase in ullage pressure. oscillations in phase with pressure oscillations at the bottom of the pool.

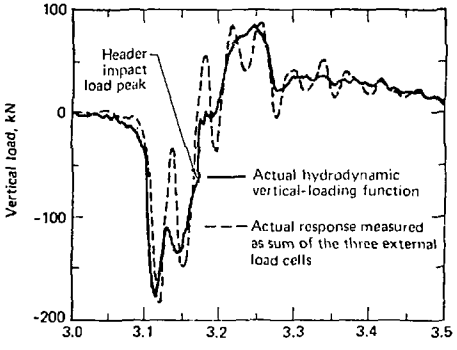


Fig. 18. [illegible] for the [illegible] 1/5-scale Pres[illegible] Suppression Experiment.

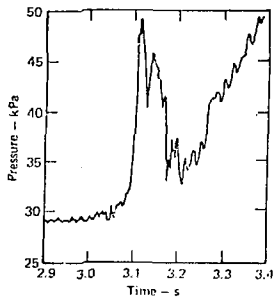


Fig. 19. Typical Pool Pressure History for the 1/5-Scale Pressure Suppression Experiment.

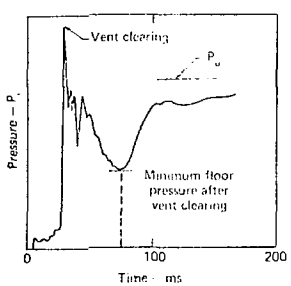


Fig. 20. Pool Pressure History from Ref. 8.

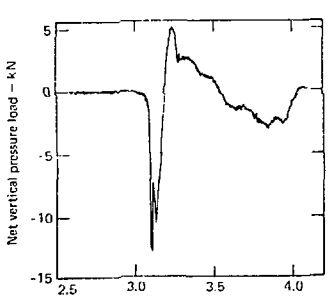


Fig. 21. Typical HVLF for the 7.5-deg. torus sector of the 1/5-Scale Pressure Suppression Experiment

ACKNOWLEDGMENTS

Appreciation is extended to the following contributors: J. Rubson, T. Schaffer, L. Trent for technical assistance in experiments. J. Caywood for instrumentation photography. Shirley A. Calvert for her inimitable, efficient preparation of the manuscript.

REFERENCES

1 McCauley, E. W., Lai, W., "BWR Mark I Pressure Suppression Study – Characterization of the Vertical Load Function Utilizing Bench Top Model Tests," UCID-17675, Feb. 1977, University of California, Lawrence Livermore Laboratory, Livermore, CA 94550.

2 Lai, W., McCauley, E. W., "Air Scaling and Modeling Studies," UCRL-52383, Oct. 1977, University of California, Lawrence Livermore Laboratory, Livermore, CA 94550.

3 McCauley, E. W., Pitts, J. H., Principal Investigators, "Bench Scale Experiments to Test Air-Water Scaling Hypotheses for the Lawrence Livermore Laboratory's 1/5-Scale BWR – Mark I Pressure Suppression Experiment Program," Progress Report UCID-17270-76-2, Dec. 1976, University of California, Lawrence Livermore Laboratory, Livermore, CA 94550

4. Lai, W., McCauley, E. W., "BWR Mark I Pressure Suppression Study – Bench Mark Experiments," UCID-17661, Jan. 1977, University of California, Lawrence Livermore Laboratory, Livermore, CA 94550.

5 Torbeck, J. E., Galyardt, D. L., and Walker, J. P., "Mark I 1/12-Scale Pressure Suppression Pool Swell Tests," NEDE-13456, March 1976, General Electric Co., Boiling Water Reactor Systems Department, San Jose, CA 95125.

6 Collins, E. K., Lai, W., ed., "Final Air Test Results for the 1/5-Scale Mark I Boiling Water Reactor Pressure Suppression Experiment, UCRL-52371, Oct. 1977, University of California, Lawrence Livermore Laboratory Livermore, CA 94550.

7 Lai, W., McCauley, E. W., "BWR Mark I Pressure Suppression Study – Effect of Downcomer Fill Level on the Vertical Load Functions," UCID-17662, Feb. 1977, University of California, Lawrence Livermore Laboratory Livermore, CA 94550.

8 Anderson, W. G., Huber, P. W., Sonin, A. A., "Modeling of Pool Swell Hydrodynamics," Progress Report, Pub. No. 77-01, March 1977 Fluid Mechanics Laboratory, Dept. of Mechanical Engineering, Massachusetts Institute of Technology, Cambridge, MA

9 Davis, B. W., "Preliminary Characterization of the Pressure Suppression Experiment Load Response and Source Analysis – Air Test Series," UCID-17552, Aug. 1977, University of California, Lawrence Livermore Laboratory, Livermore, CA 94550

10 Posehn, M. R., "Modal Analysis of the NRC Pressure Suppression Experimental Facility," UCID-17494, May 1977, University of California, Lawrence Livermore Laboratory, Livermore, CA 94550.

TABLE 1. Selected Data for Dynamic Response to Blowdown

| RUN | NOMINAL PRESS. RATIO ATM/ULLAGE | FORCE (N) | | PRESSURE (kPa) | | ACCEL ($m/s^2$) | | FREQ. (Hz) | |
|---|---|---|---|---|---|---|---|---|---|
| | | DOWN | UP | + | - | DOWN | UP | LOW | HIGH |
| V41-2 | 15/5 | 440.4 | 222.4 | - † | - † | 12.75 | 8.34 | 49 | 700 |
| V43-4 | " | 398.1 | 189.0 | - | - | 11.57 | 7.94 | 50 | 710 |
| V45-6 | " | 429.2 | 200.2 | - | - | 11.57 | 8.24 | 52 | 700 |
| V53-4 | " | 402.6 | 177.9 | - | - | 9.02 | 6.57 | 49 | 767 |
| 1/14-1 | " | 455.9 | 209.1 | 20.27 | 3.24 | 14.22 | 6.08 | 50 | 679 |
| 1/14-2 | " | 411.5 | 193.5 | 17.17 | 2.96 | 13.24 | 6.08 | 53 | 800 |
| 1/14-3 | " | 418.1 | 189.0 | 18.68 | 2.00 | 13.25 | 6.08 | 53 | 800 |
| 1/21-1 | " | 489.3 | 200.2 | 21.51 | 2.55 | --- † | ---† | 51 | 750 |
| 1/21-2 | " | 389.2 | 222.4 | 16.48 | 2.55 | ---- | ---- | 51 | 769 |
| 1/21-3 | " | 433.7 | 195.7 | 18.00 | 2.96 | ---- | ---- | 56 | --†† |
| 1/21-4 | " | 500.4 | 233.5 | 22.75 | 3.31 | 15.10 | 8.53 | 53 | 708 |
| 124-1 | " | 398.1 | 195.7 | 16.96 | 2.48 | 12.26 | 6.08 | 54 | 700 |
| | AVE | 430.5 | 202.4 | 18.98 | 2.76 | 12.55 | 7.10 | 51.8 | 734.8 |
| V47-8 | 15/7.5 | 351.4 | 177.9 | - † | - † | 10.69 | 9.02 | 59 | --- |
| V49-50 | " | 360.3 | 186.8 | - | - | 10.89 | 8.24 | 59 | 710 |
| V51-52 | " | 351.4 | 191.3 | - | - | 11.87 | 7.16 | 57 | 700 |
| V55-56 | " | 351.4 | 182.4 | - | - | 11.47 | 7.16 | 61 | 741 |
| 1/14-4 | " | 389.2 | 189.0 | 16.06 | 2.96 | 11.18 | 7.85 | 62 | --- |
| 1/14-5 | " | 355.9 | 200.2 | 17.31 | 3.65 | 11.77 | 7.35 | 59 | 714 |
| 1/21-11 | " | 322.5 | 177.9 | 14.34 | 2.55 | 10.30 | 8.92 | 62 | 750 |
| | AVE | 354.6 | 186.5 | 15.90 | 3.05 | 11.17 | 7.96 | 60 | 723.0 |
| 1/14-6 | 15/10 | 244.7 | 100.1 | 11.38 | 2.14 | 7.45 | 8.34 | 69 | 700 |
| 1/14-7 | " | 260.2 | 111.2 | 11.38 | 1.72 | 7.35 | 8.14 | 67 | --- |
| | AVE | 252.4 | 105.6 | 11.38 | 1.93 | 7.40 | 8.24 | 68 | 700 |

† Data missing because transducers not available.

†† The time scale selected for the oscilloscope caused the high frequency oscillations to be indistinct.